The Kinetics of Nucleated Polymerizations at High Concentrations: Amyloid Fibril Formation Near and Above the "Supercritical Concentration"

Evan T. Powers* and David L. Powers†
*Department of Chemistry, The Scripps Research Institute, La Jolla, California; and †Department of Mathematics and Computer Science, Clarkson University, Potsdam, New York

ABSTRACT The formation of amyloid and other types of protein fibrils is thought to proceed by a nucleated polymerization mechanism. One of the most important features commonly associated with nucleated polymerizations is a strong dependence of the rate on the concentration. However, the dependence of fibril formation rates on concentration can weaken and nearly disappear as the concentration increases. Using numerical solutions to the rate equations for nucleated polymerization and analytical solutions to some limiting cases, we examine this phenomenon and show that it is caused by the concentration approaching and then exceeding the equilibrium constant for dissociation of monomers from species smaller than the nucleus, a quantity we have named the "supercritical concentration". When the concentration exceeds the supercritical concentration, the monomer, not the nucleus, is the highest-energy species on the fibril formation pathway, and the fibril formation reaction behaves initially like an irreversible polymerization. We also derive a relation that can be used in a straightforward method for determining the nucleus size and the supercritical concentration from experimental measurements of fibril formation rates.

INTRODUCTION

Many diseases, including Alzheimer's disease, appear to be caused by the formation and deposition of a fibrillar protein aggregate known as amyloid (1–4). Amyloidogenic proteins (5,6), like other fibril-forming proteins (7), have been suggested to self-assemble by a nucleated polymerization mechanism. In a nucleated polymerization, the growth of aggregates occurs by sequential monomer addition (7–9). Monomer addition is unfavorable for species smaller than a critical size, but favorable for larger species. This critical size (n monomer units) defines the nucleus (X_n), which is the highest-energy species on the polymerization pathway (8,10–12).

Nucleated polymerizations have several well-known features according to the classical model of Oosawa and Asakura (7), including 1), a critical concentration, below which fibrils cannot form; 2), a lag phase before fibrils form, which can be eliminated by the addition of preformed fibrils (seeds); and 3), a strong dependence of the fibril formation rate on concentration, which increases with the size of the nucleus (7–9). This concentration dependence can be expressed in terms of t_{50}, the time at which a fibril formation reaction reaches 50% completion, as follows:

$$\log t_{50} = \text{constant} - \left(\frac{n+1}{2}\right)\log[X]_{\text{tot}}, \qquad (1)$$

where $[X]_{\text{tot}}$ is the total protein concentration, and n is the number of subunits in the nucleus (see Supplementary Material). Log-log plots of t_{50} (or a similar variable) versus $[X]_{\text{tot}}$ are often used in studies of amyloid or other protein fibril formation reactions (13–17) because their t_{50} values can easily be experimentally measured using dye-binding assays (18–20) or turbidimetry (21). The presence or absence of the features listed above has been important for interpreting data from in vitro amyloidogenesis experiments (13–17,22–26), which, in turn, has been important for formulating hypotheses about the pathogenesis and treatment of amyloid and other protein aggregation diseases (5,27–31). However, the classical model of nucleated polymerization cannot hold at very high concentrations. The stability of the nucleus will increase as the monomer concentration increases, and eventually, at high enough concentrations, the nucleus will be more stable than the monomer (12,32). The concentration at which this happens will be called the "supercritical concentration". As the supercritical concentration is approached and then exceeded, the features of a nucleated polymerization must become different from those listed above. Here, we report that the concentration dependence of the rate of a fibril formation reaction weakens and then nearly disappears as the concentration increases. We show that the initial weakening happens because oligomer concentrations become significant at total protein concentrations approaching the supercritical concentration, but the fibril formation reaction still behaves in most respects like a classical nucleated polymerization. Above the supercritical concentration, however, a fibril formation reaction in its early phases behaves like an irreversible polymerization, and the rate becomes almost independent of concentration as a result.

Submitted September 1, 2005, and accepted for publication March 21, 2006.

Address reprint requests to Evan T. Powers, Dept. of Chemistry, The Scripps Research Institute, La Jolla, CA 92037. E-mail: epowers@scripps.edu.

0006-3495/06/07/122/11 $2.00

doi: 10.1529/biophysj.105.073767

MATERIALS AND METHODS

Numerical integration of differential equations and other calculations were performed on a personal computer with dual AMD Athlon 2200 MP processors using Mathematica 4.2 (Wolfram Research, Champaign, IL) for Windows XP or Mathematica 5.0 for Linux.

RESULTS

Model

Fig. 1 *A* is a summary of our model for nucleated polymerization. This model contains several assumptions. First, we assumed that oligomer and fibril sizes can change only by monomer association or dissociation. Second, we assumed that the addition of monomers to the nucleus is irreversible (that is, X_{n+1} cannot lose a monomer to become X_n, so $b_{n+1} = 0$). This assumption allows us to treat all of the fibrils together, so that $[F] = [X_{n+1}] + [X_{n+2}] + \cdots + [X_N]$ is the fibril number concentration and $[M] = (n + 1)[X_{n+1}] + (n + 2)[X_{n+2}] + \cdots + N[X_N]$ is the fibril mass concentration, where $[X_i]$ is the concentration of an *i*-mer. The irreversibility of monomer addition to the nucleus has been justified by Ferrone (8) and the division of species into pre- and postnuclear aggregates (i.e., oligomers and fibrils) has been used previously in models of nucleated polymerization (7,8,33–35). Third, we have assumed that all of the association rate constants are the same ($a_1 = a_2 = a_3 = \cdots = a_N = a$), since they are largely determined by diffusion and long-range forces (36–38). Finally, we have assumed that all of the dissociation rate constants for oligomers are the same ($b_1 = b_2 = b_3 = \cdots = b_n = b$), but they decrease sharply for fibrils and stay constant thereafter ($b_{n+2} = b_{n+3} = \cdots = b_N = c < b$). The decrease in the dissociation rate constant reflects the higher stability of fibrils relative to oligomers. Our third and fourth assumptions (or similar ones) have been used previously in models of fibril formation reactions (9,12,39), but we note that Hill has shown that monomer association and dissociation constants should both depend continuously on fibril size (40).

The critical concentration can be defined in terms of the rate constants as $K_c = c/a$ (7,9,41) and the supercritical concentration as $K_s = b/a$. When $[X]_{tot} < K_c$, all polymers (fibrils as well as oligomers) are less stable than the monomer, and fibril formation cannot occur. When $K_c < [X]_{tot} < K_s$, the nucleus is the highest-energy species on the fibril formation pathway, whereas when $K_s < [X]_{tot}$, the monomer is the highest-energy species on the fibril formation pathway. These points are illustrated in Fig. 1 *B*. Our third and fourth assumptions guarantee that the size of the nucleus will not change as the concentration increases (9). This feature is most suitable for fibrils with structures in which there is a sudden change as the fibrils grow in the number or quality of interactions made. The nucleus is then determined by the size at which this sudden change occurs. This structural definition of the nucleus coincides with the thermodynamic definition (i.e., that the nucleus is the highest-energy species on the polymerization pathway) when $K_c < [X]_{tot} < K_s$, but the definitions diverge when $K_s < [X]_{tot}$. At such high protein concentrations, the thermodynamic nucleus is formally the monomer. Structural nuclei are likely to be small; it is easy to imagine a stark difference between the interactions in a tetramer and a pentamer (as in Fig. 1 *B*), but not between a 49-mer and a

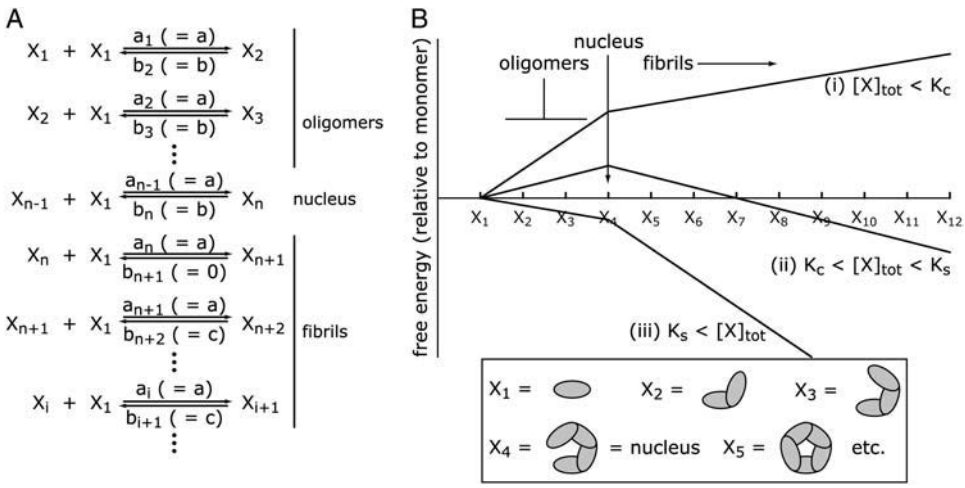

FIGURE 1 Nucleated polymerization mechanism of protein fibril formation. (*A*) The sequence of reactions in a nucleated polymerization. Aggregates are assumed to grow by monomer addition. The association and dissociation rate constants are shown above and below the arrows, respectively. The rate constants shown in parentheses arise from the assumptions in the text. The *n*-mer, X_n, is known as the nucleus. Smaller species are called oligomers, whereas larger species are called fibrils. (*B*) Plots of free energy (relative to the monomer) versus aggregate size for the formation of a helical polymer with a nucleus size of 4. Addition of a monomer to a monomer or an oligomer creates one new interaction (in the drawings below the plot, the ovals overlap in one place for X_2, X_3, and X_4). Addition of a monomer to the nucleus or a fibril creates two new interactions (the ovals overlap in two places for X_5 and all larger species). Plots are shown for total protein concentrations i), below the critical concentration; ii), between the critical and supercritical concentrations; or iii), above the supercritical concentration (where the total protein concentration is $[X]_{tot}$, the critical concentration is $K_c = c/a$, and the supercritical concentration is $K_s = b/a$; see text). Below the critical concentration, neither oligomers nor fibrils are stable relative to the monomer. Fibril formation therefore does not occur when $[X]_{tot} < K_c$. Between the critical and supercritical concentrations, oligomers are less stable than the monomer, the nucleus is the highest-energy species on the fibril formation pathway, and fibrils become stable relative to the monomer when they are large enough. Above the supercritical concentration, both oligomers and fibrils are stable relative to the monomer. Curve ii corresponds to the classical picture of a nucleated polymerization. Note that the nucleus size is independent of the concentration.

50-mer. For example, in helical fibrils (7,12,41), the number of interactions formed upon subunit addition changes when the first loop of the helix is closed (see Fig. 1 *B*). The nucleus size for helical fibrils is one less than the number of monomers in a single loop of the helix (12), which is unlikely to be large. Constant nucleus-size models have been used successfully to describe fibril formation by actin (33,34,42–46) and flagellin (47), both of which have small nuclei (three to four monomer units). They have not been useful for fibrils with larger nuclei. For example, fibril formation by hemoglobin S, which has a nucleus size on the order of 20, had to be modeled with a concentration-dependent nucleus size (10,11).

The rate equations for our nucleated polymerization model can be written using the information in Fig. 1 *A*. However, we have found it convenient to rescale the time and concentration variables as suggested by Goldstein and Stryer (9):

$$\tau = ct; \quad x_i = [X_i]/K_c; \quad f = [F]/K_c; \quad m = [M]/K_c, \quad (2)$$

where t is time. This rescaling results in time being measured relative to the monomer-fibril dissociation rate constant, and the concentrations being measured relative to the critical concentration. All of the rescaled variables are dimensionless. The rate equations, mass balance, and initial conditions for our nucleated polymerization model can be written in terms of the rescaled variables as follows (see Supplementary Material):

$$\frac{dx_1}{d\tau} = -x_1\left(2x_1 + \sum_{i=2}^{n} x_i\right) + \sigma\left(2x_2 + \sum_{i=3}^{n} x_i\right) - x_1 f + f, \quad (3)$$

$$\frac{dx_i}{d\tau} = (x_1 x_{i-1} - \sigma x_i) - (x_1 x_i - \sigma x_{i+1}), \quad 2 \le i \le n-1, \quad (4)$$

$$\frac{dx_n}{d\tau} = (x_1 x_{n-1} - \sigma x_n) - x_1 x_n, \quad (5)$$

$$\frac{df}{d\tau} = x_1 x_n, \quad (6)$$

$$\frac{dm}{d\tau} = (n+1)x_1 x_n + x_1 f - f, \quad (7)$$

$$x_{tot} = \sum_{i=1}^{n} i x_i + m, \quad (8)$$

$$x_{1,\tau=0} = x_{tot}; \quad x_{2,\tau=0} = x_{3,\tau=0} = \cdots x_{n,\tau=0} = f_{\tau=0} = m_{\tau=0} = 0, \quad (9)$$

where $\sigma = b/c = K_s/K_c$; σ is the rescaled equivalent of the supercritical concentration. Inspection of Eqs. 3–9 reveals that they cannot reach steady state, since $df/d\tau$ and $dm/d\tau$ are always >0. However, steady state can be most closely approached when $x_1 = 1$ (i.e., $[X_1] = K_c$), $x_i = 1/\sigma^{i-1}$, and, substituting these expressions into Eq. 8,

$$m = x_{tot} - \sum_{i=1}^{n} i x_i = x_{tot} - \sum_{i=1}^{n} i/\sigma^{i-1} \quad (10)$$

(see Supplementary Material). Equations 3–9 are a good model for fibril formation reactions until this near steady-state point is reached, but because f and m continue to increase after this point, the approximation breaks down at long times. We will therefore limit our use of Eqs. 3–9 to before and just after this near-steady-state point. Rescaling the time and concentration variables reduces the number of parameters to three: σ, x_{tot}, and n. Ferrone has warned, however, that rescaling can obscure whether a given value for a parameter is physically reasonable (8). The parameter ranges that will be used herein have been chosen to be appropriate for amyloid fibril formation: they are $10^2 \le \sigma \le 10^5$, $x_{tot} \le 10^6$, and $3 \le n \le 9$. These parameter ranges are justified in the Supplementary Material.

Limiting cases

We examine two limiting cases here. The first is that of a classical nucleated polymerization. The features of a classical nucleated polymerization (in particular, the high concentration dependence of the rate) are well known and have already been mentioned in the Introduction. We merely wish to add here that classical nucleated polymerizations require the following conditions to be met: 1), the monomer must quickly come to a preequilibrium with oligomers, so that the nucleation rate is dictated by the relative stabilities of the nucleus and monomer; 2), the oligomer concentrations must be low enough to be ignored relative to the monomer concentration ($x_i \ll x_1$, $2 \le i \le n$); and 3), the initial monomer concentration must be high enough for monomer dissociation from fibrils to be negligible throughout most of the fibril formation reaction. The first two conditions are met when $x_{tot} \ll \sigma$ and the third is met when $1 \ll x_{tot}$, so this limiting case obtains when $1 \ll x_{tot} \ll \sigma$. The rate equations (Eqs. 3–9) can be simplified for a classical nucleated polymerization and solved analytically (7) (see Supplementary Material). We show the solutions for x_1, f, and m here (since they will be used later):

$$x_1 = x_{tot}\left[\operatorname{sech}\left(\tau\sqrt{\frac{(n+1)x_{tot}^{n+1}}{2\sigma^{n-1}}}\right)\right]^{\frac{2}{n+1}}, \quad (11)$$

$$f = \sqrt{\frac{2x_{tot}^{n+1}}{(n+1)\sigma^{n-1}}}\tanh\left(\tau\sqrt{\frac{(n+1)x_{tot}^{n+1}}{2\sigma^{n-1}}}\right), \quad (12)$$

$$m = x_{tot}\left\{1 - \left[\operatorname{sech}\left(\tau\sqrt{\frac{(n+1)x_{tot}^{n+1}}{2\sigma^{n-1}}}\right)\right]^{\frac{2}{n+1}}\right\}. \quad (13)$$

Equation 13 allows the constant in Eq. 1 to be expressed in terms of the parameters n and σ. Monomer dissociation from fibrils is ignored in classical nucleated polymerizations (because of the third condition listed above), so $m = x_{tot}$ at completion and therefore $m = 0.5x_{tot}$ at τ_{50}. Inserting

$m = 0.5x_{tot}$ into Eq. 13, solving for τ_{50}, inserting the solution into Eq. 1, and converting from t_{50} and $[X]_{tot}$ to τ_{50} and x_{tot} yields

$$\log_{10}\tau_{50} = \log_{10}\left[\sqrt{\frac{2\sigma^{n-1}}{n+1}}\,\mathrm{sech}^{-1}(0.5^{(n+1)/2})\right] - \left(\frac{n+1}{2}\right)\log_{10}x_{tot}. \quad (14)$$

Equation 14 shows that the value of τ_{50} for a classical nucleated polymerization can be determined at any value of x_{tot} if n and σ are known.

Our second limiting case is that of very high concentrations. Monomer dissociation from both fibrils and oligomers can be ignored when the protein concentration is high enough ($x_{tot} \gg \sigma$) (9). Thus, this limiting case corresponds to an irreversible polymerization. The rate equations for an irreversible polymerization can be solved analytically (see Supplementary Material), yielding

$$x_i = x_{tot}e^{-s}\left(\frac{s^{i-1}}{(i-1)!} - \frac{s^i}{i!}\right), \quad i \geq 1, \quad (15)$$

where s is a concentration-time integral (48,49)

$$s = \int_0^{\tau'} x_1 \quad d\tau. \quad (16)$$

Goldstein and Stryer have also obtained Eq. 15 for the special case $i = 1$ (9). Solutions for x_i in terms of τ could in principle be obtained by inverting Eq. 16, but this yields an exponential integral:

$$\tau = \frac{1}{x_{tot}}\int_0^s \frac{e^{s'}}{1-s'}ds'. \quad (17)$$

Equation 17 can only be integrated numerically, but inspection reveals that $\tau \to \infty$ as $s \to 1$, which implies that the reaction is complete at $s = 1$. The concentration of the monomer at this point, the end of the reaction, is 0, whereas the concentrations of the other species are:

$$x_{i,s=1} = x_{i,\tau\to\infty} = x_{tot}e^{-1}\frac{i-1}{i!}. \quad (18)$$

Fig. 2 *A* is a plot of the weight fractions (ix_i/x_{tot}) of monomers to hexamers over the course of an irreversible polymerization. Fig. 2 *B* is a plot of weight fractions at the end of an irreversible polymerization against aggregate size. (Weight fractions are plotted instead of concentrations because they are independent of x_{tot}; see Eqs. 15 and 18). Fig. 2 shows that species larger than hexamers are always negligible (weight fraction <0.01 for all τ for $i > 6$) and that dimers, trimers, and (to a lesser extent) tetramers are the dominant species at the end of an irreversible polymerization. It should be noted that experimental fibril formation reactions can behave like irreversible polymerizations only while the monomer concentration is high. Eventually, when the monomer concentration is low enough and oligomer concentrations are high enough, monomer dissociation will no longer be negligible. The fibril formation reaction will then relax from the (oligomer-rich) state it is in when monomer dissociation can no longer be ignored to the near-steady-state point (where fibrils dominate). The effect of fibril formation reactions obeying the kinetics of irreversible polymerizations early in their time courses does not manifest itself in the distribution of products at the end of the reaction, but in the concentration dependence of the fibril formation rate. This point will be discussed further below.

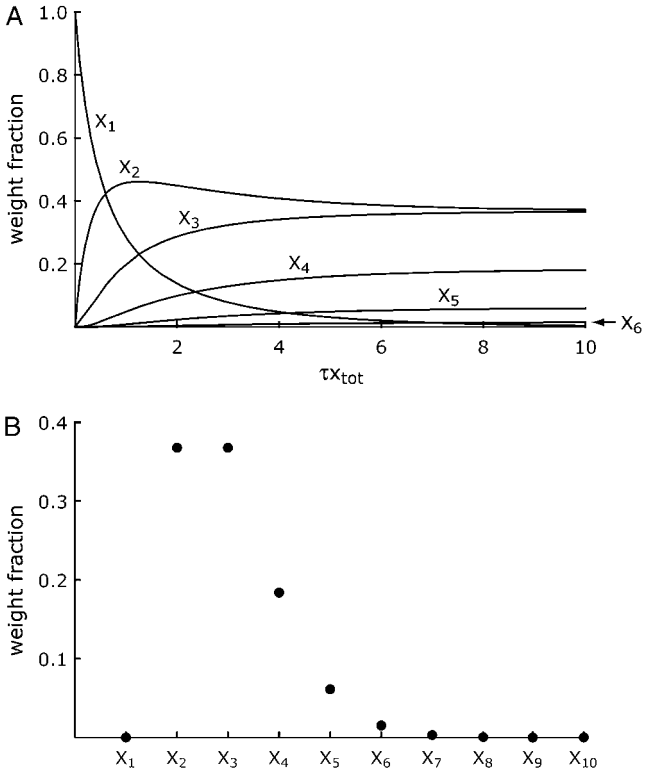

FIGURE 2 (*A*) Time courses of the weight fractions of the monomer (X_1), dimer (X_2), trimer (X_3), tetramer (X_4), pentamer (X_5), and hexamer (X_6) in an irreversible polymerization. The plots were made using Eqs. 15 and 17. The quantity τx_{tot} is used for the time variable because τ is inversely proportional to x_{tot} (see Eq. 17), so using τx_{tot} for the independent variable enables the weight fraction plots to be independent of x_{tot}. (*B*) A plot of weight fraction versus species size at the end of an irreversible polymerization.

Concentration dependence of fibril formation reaction rates: a test case

Some insight into the behavior of nucleated polymerizations can be gained by studying a representative test case. Equations 3–9 were therefore solved numerically with $n = 6$, $\sigma = 1000$, and x_{tot} varying from $10^{0.25}$ to 10^6 in steps of $10^{0.25}$. Fig. 3 *A* is a plot of the fraction completion, defined as the fibril mass concentration at a given time divided by the fibril mass concentration at the near-steady-state point (given

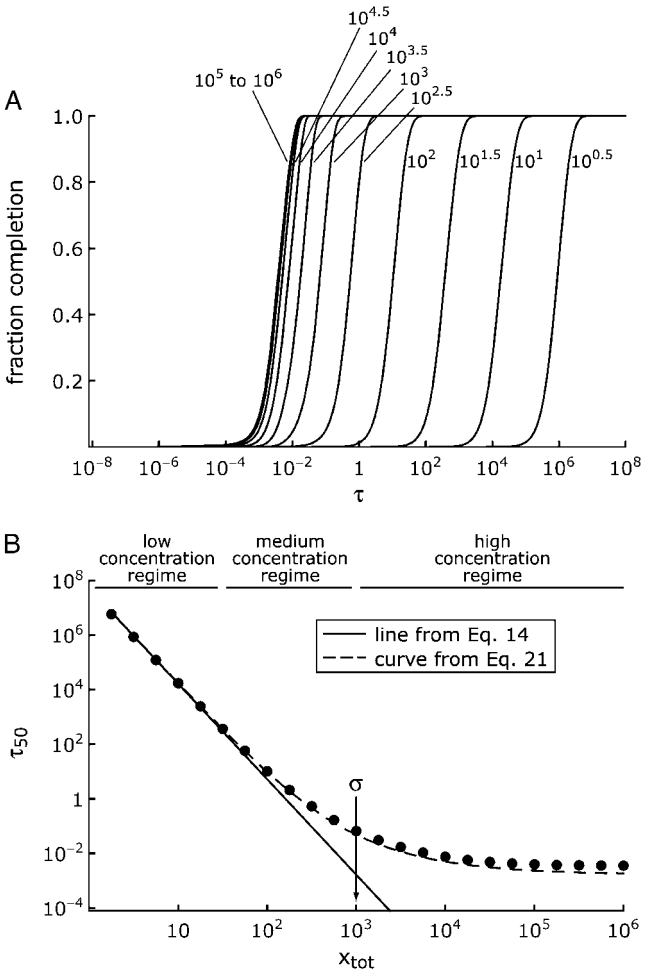

FIGURE 3 (*A*) Plots of the fraction completion versus rescaled time (τ) on a logarithmic scale for the test case with $n = 6$, $\sigma = 1000$, and selected values of x_{tot}. The fraction completion is defined as m/m_{final}, where m_{final} is the value of m at the near-steady-state point (see Eq. 10). Fraction completion was calculated using the numerical solutions of Eqs. 3–9. Each curve is labeled with its corresponding value of x_{tot}. As mentioned in the text, the curves for $x_{tot} = 10^5$–10^6 are nearly identical to each other. (*B*) A plot of the rescaled time required for a fibril formation reaction to reach 50% completion (τ_{50}) against the total protein concentration (x_{tot}), with both variables on a logarithmic scale for the test case with $n = 6$ and $\sigma = 1000$. The solid circles represent the τ_{50} values obtained from the numerical solutions of Eqs. 3–9, the solid line represents the τ_{50} values expected for a classical nucleated polymerization (Eq. 14), and the dashed curve represents the τ_{50} values expected for a classical nucleated polymerization after correcting for oligomer formation (Eq. 21).

by Eq. 10), against τ (on a logarithmic scale) for selected values of x_{tot}. Fig. 3 *B* is a log-log plot of the values of τ_{50} from the numerical solutions versus x_{tot}. Fig. 3 shows that the concentration dependence of fibril formation kinetics changes as the concentration increases, as has also been observed by Kodaka (39). Three concentration regimes (low, medium, and high) can be identified based on the relative values of the total protein concentration (x_{tot}) and the supercritical concentration (σ). In the low-concentration regime, where x_{tot} is much less than σ ($x_{tot} \leq 10^{1.5}$), the time courses in Fig. 3 *A* are evenly spaced and the τ_{50} vs. x_{tot} log-log plot in Fig. 3 *B* is linear. In fact, these τ_{50} values are very close (within 0.1 $\log_{10}$ unit) to the solid line in Fig. 3 *B*, which represents the τ_{50} values expected for a classical nucleated polymerization (the solid line was plotted using Eq. 14). In the medium-concentration regime, where x_{tot} is closer to, but still less than, σ ($10^{1.5} < x_{tot} \leq \sigma = 10^3$), the fraction completion plots become increasingly closely spaced in Fig. 3 *A* and the τ_{50} values deviate from the solid line in Fig. 3 *B* (although they still fall on the dashed curve, the origin of which is explained below). The curvature in the log-log plot of τ_{50} vs. x_{tot} shows that the fibril formation reaction does not meet the requirements of classical nucleated polymerizations in the medium-concentration regime. In the high-concentration regime, where $x_{tot} > \sigma$, the fraction completion plots in Fig. 3 *A* are almost identical, and τ_{50} is nearly independent of x_{tot} when $x_{tot} \geq 10^5$ in Fig. 3 *B* (τ_{50} changes by <0.05 log units between $x_{tot} = 10^5$ and 10^6). This behavior marks an even more serious departure from classical nucleated polymerization.

The concentration dependence of fibril formation for this test case can be understood by using the information in Fig. 4. Fig. 4 is a comparison of the numerical solutions of Eqs. 3–9 to the solutions of a classical nucleated polymerization at $x_{tot} = 10$ (Fig. 4 *A*) or 100 (Fig. 4 *B*), or to the solutions of an irreversible polymerization at $x_{tot} = 10^5$ (Fig. 4 *C*). The values of x_{tot} used in Fig. 4 represent the low, medium, and high-concentration regimes. Three phases in the fibril formation reaction can be identified in the low and medium-concentration regimes. In the first phase (preequilibration), the monomer quickly reaches preequilibrium with oligomers and the nucleus. In the second phase (nucleation), nucleation takes place at a constant nucleus concentration, and therefore at a constant rate. In the third phase (conversion), monomer is converted to fibrils. The fibril formation reaction ends when the monomer concentration is equal to the critical concentration ($x_1 = 1$), at which point the reaction is at the near-steady-state point. There is, however, an important difference between the fibril formation time courses in the low and medium-concentration regimes. In the low-concentration regime, where the total protein concentration is well below the supercritical concentration, the fibril formation reaction meets the requirements for a classical nucleated polymerization: the monomer reaches preequilibrium almost instantaneously (by $\tau = 10^{-2}$), the concentrations of oligomers are low ($<2\%$ of x_{tot}), and $x_{tot} \gg 1$ throughout most of the reaction. This assertion is supported by the similarity between the numerical solutions of Eqs. 3–9 (*solid curves*) and the classical nucleated polymerization solutions (*dashed curves*) in Fig. 4 *A*. These solutions deviate only near the end of the conversion phase (and only because monomer dissociation from fibrils is not accounted for in classical nucleated polymerizations). In contrast, substantial amounts of oligomers form during the preequilibration phase in the medium-concentration regime ($>15\%$ of the total

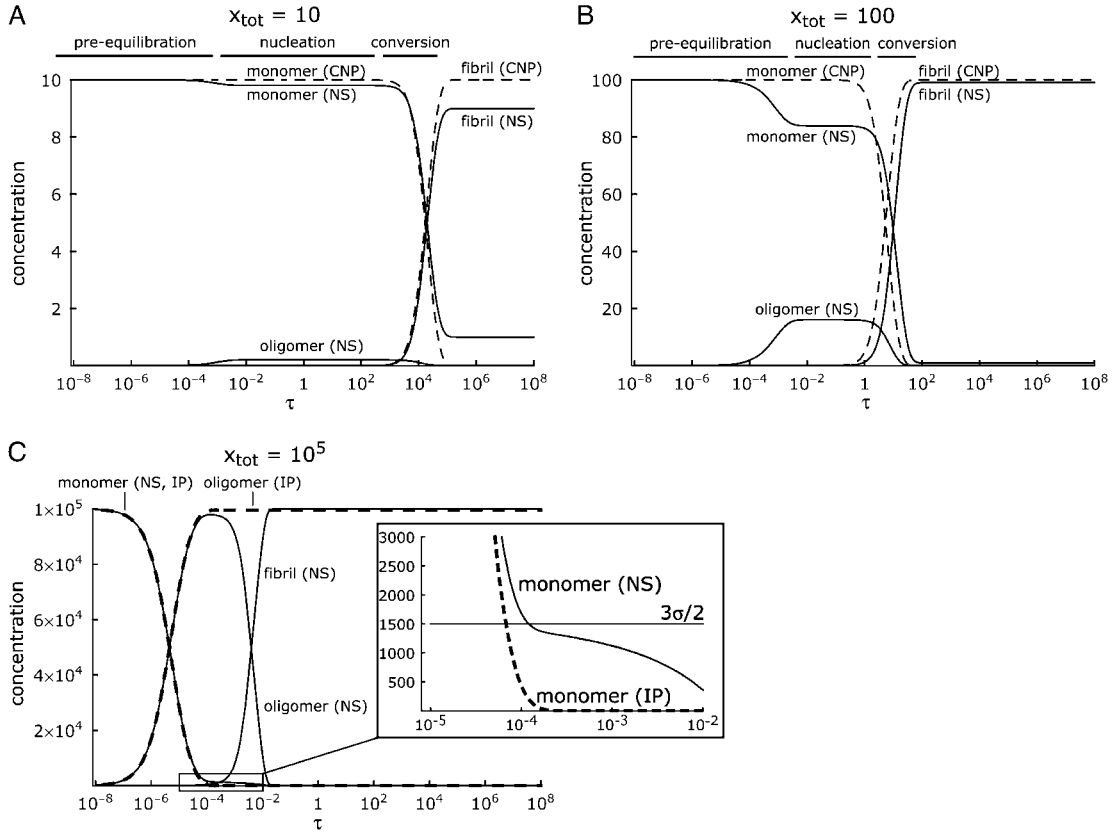

FIGURE 4 (*A*) Plots of monomer, oligomeric protein, and fibril mass concentrations versus rescaled time (τ) on a logarithmic scale for the test case with $n = 6$ and $\sigma = 1000$ in the low-concentration regime ($x_{tot} = 10$; the oligomeric protein concentration is defined as $2x_2 + 3x_3 + \ldots + nx_n$). The solid lines represent the time courses from the numerical solutions (*NS*) to the rate equations. The dashed lines represent the time courses expected for a classical nucleated polymerization (*CNP*). The three phases of the fibril formation reaction, preequilibration, nucleation, and conversion, are marked above the plots. (*B*) As in *A*, except that the plots are for the medium-concentration regime ($x_{tot} = 100$). (*C*) Plots of monomer, oligomeric protein, and fibril mass concentrations versus rescaled time (τ) on a logarithmic scale for the test case with $n = 6$ and $\sigma = 1000$ in the high-concentration regime ($x_{tot} = 10^5$). The solid lines represent the time courses from the numerical solutions (*NS*) to the rate equations. The dashed lines represent the time courses expected for an irreversible polymerization (*IP*). (*Inset*) An expansion of the monomer concentration time course between $10^{-5} < \tau < 10^{-2}$.

amount of protein when $x_{tot} = 100$; see Fig. 4 *B*), where the total protein concentration is closer to the supercritical concentration. This degree of oligomer formation violates the second requirement of classical nucleated polymerizations. It causes the monomer concentration to be $<x_{tot}$ during the nucleation phase, which lowers the nucleus concentration, which in turn decreases the fibril nucleation rate and slows the fibril formation reaction. This point is illustrated by the deviation of the numerical solutions (*solid curves*) from the classical nucleated polymerization solutions (*dashed curves*) in Fig. 4 *B*, and by the deviation of τ_{50} from the theoretical line at $x_{tot} = 100$ in Fig. 3 *B*. This deviation increases as x_{tot} approaches σ.

Although the fibril formation reaction in the medium-concentration regime does not meet the second condition for classical nucleated polymerizations, preequilibrium between the monomer and oligomeric protein is quickly attained, which meets the first, and $x_{tot} \gg 1$, which meets the third (see Fig. 4 *B*). These observations suggest that fibril formation in the medium-concentration regime can still be understood within the framework of classical nucleated polymerizations. In particular, Eq. 14 can still be used to calculate τ_{50} values for fibril formation if x_{tot} is replaced with the concentration of monomer that actually exists during the nucleation phase. The actual monomer concentration can be determined by noting that at preequilibrium $x_i = x_1^i/\sigma^{i-1}$ (see Supplementary Material) and the fibril mass concentration should be negligible ($m \approx 0$). The conservation of mass (Eq. 8) then becomes

$$x_{tot} = \sum_{i=1}^{n} ix_i + m \approx \sum_{i=1}^{n} ix_i = \sum_{i=1}^{n} \frac{ix_1^i}{\sigma^{i-1}} \approx \frac{x_1\sigma^2}{(x_1 - \sigma)^2}. \quad (19)$$

The relevant root of Eq. 19 is

$$x_1 = \frac{\sigma(2x_{tot} + \sigma - \sqrt{4\sigma x_{tot} + \sigma^2})}{2x_{tot}}. \quad (20)$$

Equation 20 is accurate to $<5\%$ for $n \geq 4$ and $x_{tot} \leq \sigma$. The error is $>10\%$ only when $n = 3$ and $x_{tot} > 0.97\sigma$. Note

that $x_1 \rightarrow x_{tot}$ at preequilibrium when $x_{tot} \ll \sigma$. Replacing x_{tot} in Eq. 14 with the expression on the right-hand side of Eq. 20 yields

$$\log_{10}\tau_{50} = \log_{10}\left[\sqrt{\frac{2\sigma^{n-1}}{n+1}}\,\mathrm{sech}^{-1}(0.5^{(n+1)/2})\right] - \left(\frac{n+1}{2}\right)\log_{10}\left[\frac{\sigma(2x_{tot}+\sigma-\sqrt{4\sigma x_{tot}+\sigma^2})}{2x_{tot}}\right]. \quad (21)$$

Equation 21 is plotted as the dashed curve in Fig. 3 *B*. This curve deviates from the numerically calculated τ_{50} values by <0.15 log units between $x_{tot} = 10^{0.25}$ and 10^3. The closeness of this fit justifies the assertion made above that the test case still behaves like a classical nucleated polymerization in the medium-concentration regime, except for the amount of oligomers formed. The dashed curve in Fig. 3 *B*, however, still deviates from the τ_{50} values in the high-concentration regime.

As in the medium-concentration regime, a large amount of oligomeric protein quickly forms in the high-concentration regime (>97% of the total by $\tau = 10^{-4}$ at $x_{tot} = 10^5$). Furthermore, preequilibrium between monomer and oligomers is never attained, as illustrated by the lack of a plateau in the oligomer concentration in Fig. 4 *C*. These two observations indicate that neither the first nor the second requirement for a classical nucleated polymerization is met by fibril formation reactions in the high-concentration regime, and it is therefore unlikely that the classical nucleated polymerization framework will be useful in understanding their behavior. In contrast, the coincidence of the numerical solutions of the rate equations (*solid curves*) and the irreversible polymerization solutions (*dashed curves*) in Fig. 4 *C* shows that the irreversible polymerization model accurately predicts fibril formation kinetics until the monomer concentration becomes small enough that dissociation reactions are no longer negligible ($\tau \approx 10^{-4}$). This similarity to an irreversible polymerization can be used to explain the near-independence of τ_{50} and x_{tot} in the high-concentration regime as follows.

Fibril formation reactions at high concentrations behave initially like irreversible polymerizations because association reactions dominate dissociation reactions ($x_1x_i \gg \sigma x_i$ for all i). However, the monomer concentration decreases as fibril formation proceeds, allowing monomer dissociation reactions to become more and more significant. Eventually the association and dissociation rates balance. This point is illustrated in the inset to Fig. 4 *C*, which shows that the monomer concentration reaches a gently sloping plateau at $x_1 \approx 1500$, or $3\sigma/2$. It can be shown (see Supplementary Material) that the same happens at higher concentrations with the plateau always being close to $3\sigma/2$, no matter what x_{tot} is. When x_1 reaches its plateau, the concentrations of dimers, trimers, etc. are close to the concentrations expected at the end of an irreversible polymerization (see Supplementary Material). As a result, the concentrations of oligomers are directly proportional to x_{tot} (see Eq. 18). Now, the time required for the fibril formation reaction to proceed from the point at which x_1 has reached its plateau to completion depends on the magnitudes of the individual terms in the rate equations relative to the total amount of protein that has to be converted into fibrils. Almost all of the terms in Eqs. 3–7 have the form x_1x_i or σx_i. Since x_1 is independent of x_{tot} once it reaches its plateau and x_i is directly proportional to x_{tot} for all $i \geq 2$, these terms are directly proportional to x_{tot}. In other words, the terms in the rate equations increase in direct proportion to the amount of protein that has to be converted into fibrils. Therefore, in the high-concentration regime, the time required to convert the protein into fibrils remains roughly constant as the protein concentration increases. In fact, it can be shown that

$$\tau_{50} \approx \frac{\ln 0.5}{-\left(\frac{5\sigma}{2}-\frac{\sigma-1}{n!}\right)+2\cos(\pi/n)\sqrt{\sigma\left(\frac{3\sigma}{2}-\frac{\sigma-1}{n!}\right)}} \quad (22)$$

is a reasonable, if rough, approximation for the asymptotic value of τ_{50} at extremely high concentrations. Equation 22 is accurate to within a factor of ~4, depending on n and σ (see Supplementary Material). Note that the parameter n in Eq. 22 does not represent the size of the thermodynamic nucleus, since the monomer is the ''nucleus'' in the high-concentration regime. Instead, n represents the size of the structural nucleus, that is, the size of the species that would be the nucleus if the protein concentration were less than the supercritical concentration.

Our assumption that species grow only by monomer addition, which is crucial to the results described above, may not be physically realistic in the high-concentration regime. Because oligomers are abundant during fibril formation in the high-concentration regime (Fig. 4 *C*), there is no reason to expect that they will not associate with each other. If oligomer-oligomer association occurred, the fibril formation reaction would have the same kinetics as colloidal aggregation, as first described by von Smoluchowski (50,51). Fibril formation models in which oligomer-oligomer associations occur are beyond the scope of this work, but Kodaka has shown that, under these circumstances, the rate of fibril formation would be inversely proportional to the total protein concentration (39).

Concentration dependence of fibril formation rates for $3 \leq n \leq 9$ and $10^2 \leq \sigma \leq 10^5$

Fig. 5 is composed of log-log plots of τ_{50} against x_{tot} for several values of n and σ. Each plot contains τ_{50} values calculated from the numerical solutions to the rate equations for a range of total protein concentrations ($x_{tot} \leq 10^6$), for

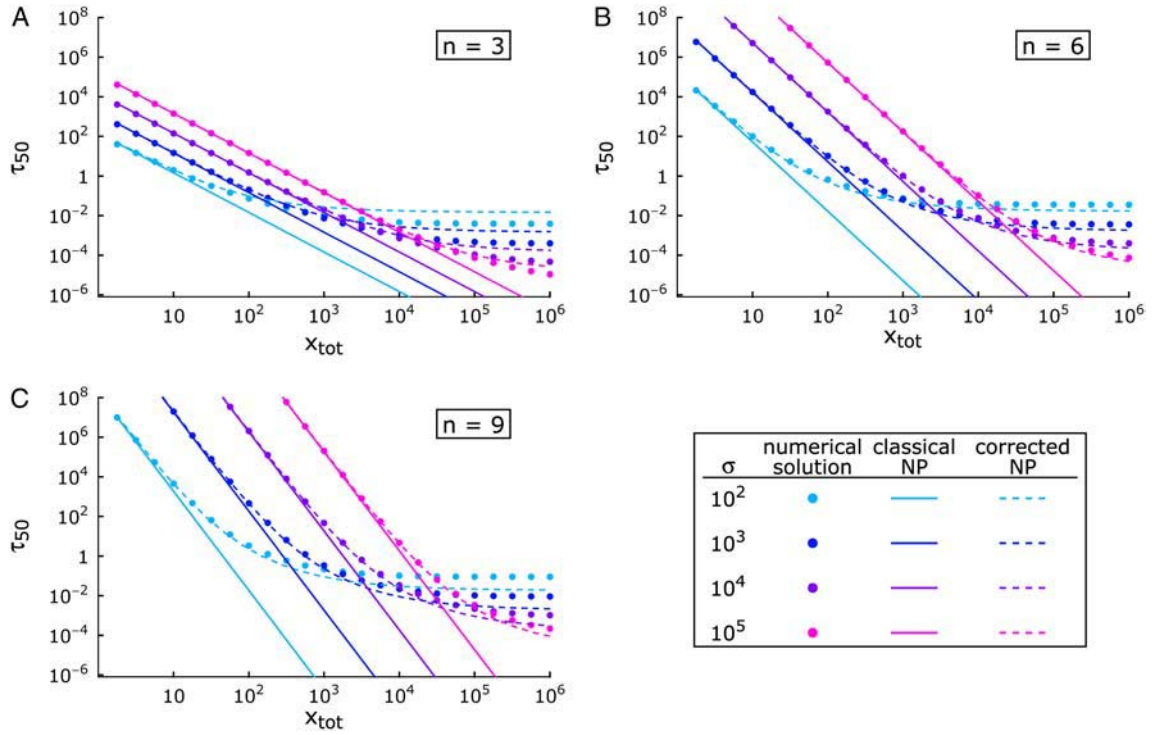

FIGURE 5 Log-log plots of the rescaled time required for a fibril formation reaction to reach 50% completion (τ_{50}) against the total protein concentration (x_{tot}). Data for several values of n and σ are shown. The solid circles represent the τ_{50} values obtained from the numerical solutions of the rate equations, the solid lines represent the τ_{50} values expected from a classical nucleated polymerization (*classical NP*), and the dashed curves represent the τ_{50} values expected from a classical nucleated polymerization after correcting for oligomer formation (*corrected NP*). The colors of the solid circles, solid lines, and dashed curves correspond to the values of σ as shown in the key in the lower right, and each graph shows data for a single value of n. (*A*) $n = 3$; (*B*) $n = 6$; and (*C*) $n = 9$.

four values of σ ($\sigma = 10^2$, 10^3, 10^4, and 10^5) at a given value of n ($n = 3$, 6, or 9). The behavior observed in the test case described above is evident in the plots in Fig. 5. The τ_{50} values (*solid circles*) are close to the values expected for a classical nucleated polymerization in the low-concentration regime ($x_{tot} \ll \sigma$; *solid lines*). They deviate from classical behavior in the medium-concentration regime ($x_{tot} < \sigma$), but still are close to the values expected for a nucleated polymerization after correction for oligomer formation (*dashed curves*). Finally, the τ_{50} values deviate from both of these approximations in the high-concentration regime ($x_{tot} > \sigma$), becoming nearly constant at very high concentrations. It is noteworthy that the fastest fibril formation reactions occur when both σ and x_{tot} are very large (compare the τ_{50} values at $x_{tot} = 10^6$ for the cases in which $\sigma = 10^2$ and 10^5 for any nucleus size). This finding is, perhaps, counterintuitive, because high values of σ should result in low nucleus concentrations and slow fibril formation rates. However, fast fibril formation reactions require not only high nucleus concentrations, but also high monomer concentrations (because the rate of fibril nucleation is the product of the concentrations of these two species, and the rate of fibril elongation is proportional to the monomer concentration). As shown in the preceding section, the monomer concentration quickly reaches a plateau value close to $3\sigma/2$ in the high-concentration regime. Larger values of σ therefore lead to higher monomer concentrations and faster fibril formation.

DISCUSSION

The kinetics of nucleated polymerizations at high concentrations

Our results demonstrate that fibril formation reactions with the mechanism in Fig. 1 *A*, including amyloid fibril formation, behave differently as the total protein concentration changes relative to the supercritical concentration. This difference in behavior manifests itself in log-log plots of τ_{50} vs. x_{tot}. These plots start as straight lines in the low-concentration regime (protein concentration $\ll$ supercritical concentration), as expected from the classical picture of nucleated polymerizations. The plots become curved in the medium-concentration regime (protein concentration $<$ supercritical concentration), and eventually become flat lines in the high-concentration regime (protein concentration $>$ supercritical concentration). These findings should be borne in mind when interpreting experimental data from fibril formation reactions; the mechanism shown in Fig. 1 *A* should not be dismissed only because log-log plots of experimental t_{50} values versus total protein concentration are found to be

curved. In fact, as discussed below, useful information can be extracted from such data.

Connection to experiment

Log-log plots of τ_{50} vs. x_{tot} should be accurately described by Eq. 14 when $1 \ll x_{tot} \ll \sigma$ and by Eq. 21 when x_{tot} is closer to, but still less than, σ. Relationships like those in Eqs. 14 and 21 can be established for the experimentally relevant unrescaled quantities, t_{50}, $[X]_{tot}$, and K_s:

$$\log_{10} t_{50} = Q - \frac{n+1}{2}\log_{10}[X]_{tot} \quad \text{for} \quad K_c \ll [X]_{tot} \ll K_s, \tag{23}$$

$$\log_{10} t_{50} = Q - \frac{n+1}{2} \times \log_{10}\left[\frac{K_s(2[X]_{tot} + K_s - \sqrt{4K_s[X]_{tot} + K_s^2})}{2[X]_{tot}}\right], \quad \text{for} \quad [X]_{tot} < K_s, \tag{24}$$

where Q is a constant. Fits of Eqs. 23 and 24 to log-log plots of t_{50} vs. $[X]_{tot}$ can be used in principle to determine n and possibly K_s, both of which are important for characterizing a nucleated polymerization. Whether these parameters can be accurately estimated in practice depends on the level of error in the t_{50} measurements, the breadth of the concentration range for which t_{50} values were experimentally measured, and the location of this concentration range relative to the supercritical concentration. We suggest the following guidelines for the use of Eq. 24: the standard error in the measured t_{50} values should be <0.3 log units (about a factor of 2); the t_{50} values should be measured over at least a 30-fold concentration range; and the protein concentration should be close enough to the supercritical concentration for there to be noticeable curvature in the log-log plot of t_{50} vs. $[X]_{tot}$. If the plot is not curved, Eq. 23 instead of Eq. 24 should be fit to the t_{50} data. Finally, if the plot is flat (i.e., t_{50} is nearly independent of $[X]_{tot}$), then neither Eq. 23 nor Eq. 24 should be fit to the data.

Good fits of Eqs. 23 and 24 to experimental t_{50} data that yield physically reasonable estimates of n and K_s are evidence that a fibril formation reaction is a nucleated polymerization, but independent tests are always desirable. Examination of the time course of a fibril formation reaction can provide such a test. Ferrone has shown that the early portion of nucleated polymerization time courses (the first 10–20%) are well described by the expression

$$[M] = A[1 - \cos(Bt)], \tag{25}$$

where A and B are adjustable parameters (8,10,11,34). We have found empirically that Eq. 25 fits the first 10% of the time courses of nucleated polymerizations in all concentration regimes (data not shown). In contrast, Eq. 25 does not fit the time courses of fibril formation reactions that have other mechanisms (for example, those in which fibril fragmentation or heterogeneous nucleation are important secondary pathways for the formation of new fibrils) (8,10,11,34). Thus, if Eq. 25 fits the time courses of the fibril formation reactions of a given protein and Eq. 23 or 24 fits the log-log plot of t_{50} vs. $[X]_{tot}$, it can reasonably be concluded that the protein forms fibrils by a nucleated polymerization mechanism and estimates obtained for n and/or K_s can be considered valid.

The effect of variable nucleus sizes

The findings described in the previous sections are most relevant to fibril formation reactions in which the nucleus size is constant, but they also have some relevance to fibril formation reactions in which the nucleus size depends on concentration. As we have argued above, in constant-nucleus-size-models, oligomers become more stable as the concentration increases, which causes log-log plots of τ_{50} vs. x_{tot} to be curved. In variable-nucleus-size models, the nucleus size will change in addition to oligomers becoming more stable as the concentration increases. The curvature in log-log plots of τ_{50} vs. x_{tot} for variable-nucleus-size models therefore should be even more pronounced than it is for constant-nucleus-size models. At very high concentrations, the nucleus ceases to be the highest energy species on the fibril formation pathway in both types of models. Fibril formation reactions will initially behave like irreversible polymerizations when the concentration is well above the supercritical concentration, and t_{50} values will be independent of the total protein concentration, no matter what type of model is used for nucleation.

CONCLUSIONS

The behavior of a nucleated polymerization reaction depends on concentration. When the protein concentration is low relative to the supercritical concentration, the classical behavior described by Oosawa and Asakura is observed (7). When the protein concentration is close to (but not greater than) the supercritical concentration, the dependence of the time required for the reaction on the protein concentration weakens, but this can be corrected for simply by accounting for the amount of monomer that forms oligomers during the nucleation phase. The reaction retains the essential features of a nucleated polymerization. However, when the protein concentration is greater than the supercritical concentration, the time required for the reaction becomes almost independent of the protein concentration and the reaction resembles an irreversible polymerization at early times. This drastic change in behavior occurs because the monomer, not the nucleus, is the highest-energy species on the fibril formation pathway. The different behavior of nucleated polymerizations at different protein concentrations must be borne in mind when assigning mechanisms based on experimental data.

SUPPLEMENTARY MATERIAL

An online supplement to this article can be found by visiting BJ Online at http://www.biophysj.org.

We thank Jeffery W. Kelly and Joel N. Buxbaum for helpful discussions.

REFERENCES

1. Sipe, J. D. 1994. Amyloidosis. *Crit. Rev. Clin. Lab. Sci.* 31:325–354.
2. Sipe, J. D., and A. S. Cohen. 2000. Review: history of the amyloid fibril. *J. Struct. Biol.* 130:88–98.
3. Selkoe, D. J. 2003. Folding proteins in fatal ways. *Nature*. 426: 900–904.
4. Dobson, C. M. 2003. Protein folding and misfolding. *Nature*. 426: 884–890.
5. Jarrett, J. T., and P. T. Lansbury. 1993. Seeding one-dimensional crystallization of amyloid: a pathogenic mechanism in Alzheimer's disease and scrapie. *Cell*. 73:1055–1058.
6. Harper, J. D., and P. T. Lansbury, Jr. 1997. Models of amyloid seeding in Alzheimer's disease and scrapie: mechanistic truths and physiological consequences of the time-dependent solubility of amyloid proteins. *Annu. Rev. Biochem.* 66:385–407.
7. Oosawa, F., and S. Asakura. 1975. Thermodynamics of the polymerization of protein. Academic Press, London.
8. Ferrone, F. 1999. Analysis of protein aggregation kinetics. *Methods Enzymol.* 309:256–274.
9. Goldstein, R. F., and L. Stryer. 1986. Cooperative polymerization reactions: analytical approximations, numerical examples, and experimental strategy. *Biophys. J.* 50:583–599.
10. Ferrone, F. A., J. Hofrichter, and W. A. Eaton. 1985. Kinetics of sickle hemoglobin polymerization. 1. Studies using temperature-jump and laser photolysis techniques. *J. Mol. Biol.* 183:591–610.
11. Ferrone, F. A., J. Hofrichter, and W. A. Eaton. 1985. Kinetics of sickle hemoglobin polymerization. 2. A double nucleation mechanism. *J. Mol. Biol.* 183:611–631.
12. Firestone, M. P., R. Delevie, and S. K. Rangarajan. 1983. On one dimensional nucleation and growth of living polymers. 1. Homogeneous nucleation. *J. Theor. Biol.* 104:535–552.
13. Arvinte, T., A. Cudd, and A. F. Drake. 1993. The structure and mechanism of formation of human calcitonin fibrils. *J. Biol. Chem.* 268:6415–6422.
14. Serio, T. R., A. G. Cashikar, A. S. Kowal, G. J. Sawicki, J. J. Moslehi, L. Serpell, M. F. Arnsdorf, and S. L. Lindquist. 2000. Nucleated conformational conversion and the replication of conformational information by a prion determinant. *Science*. 289:1317–1321.
15. Sokolowski, F., A. J. Modler, R. Masuch, D. Zirwer, M. Baier, G. Lutsch, D. A. Moss, K. Gast, and D. Naumann. 2003. Formation of critical oligomers is a key event during conformational transition of recombinant Syrian hamster prion protein. *J. Biol. Chem.* 278:40481–40492.
16. Hurshman, A. R., J. T. White, E. T. Powers, and J. W. Kelly. 2004. Transthyretin aggregation under partially denaturing conditions is a downhill polymerization. *Biochemistry*. 43:7365–7381.
17. Frankenfield, K. N., E. T. Powers, and J. W. Kelly. 2005. Influence of the N-terminal domain on the aggregation properties of the prion protein. *Protein Sci.* 14:2154–2166.
18. LeVine, H. 1999. Quantification of β-sheet amyloid fibril structures with thioflavin T. *Methods Enzymol.* 309:274–284.
19. Klunk, W. E., R. F. Jacob, and R. P. Mason. 1999. Quantifying amyloid by Congo red spectral shift assay. *Methods Enzymol.* 309:285–305.
20. Naiki, H., and F. Gejyo. 1999. Kinetic analysis of amyloid fibril formation. *Methods Enzymol.* 309:305–318.
21. Andreu, J. M., and S. N. Timasheff. 1986. The measurement of cooperative protein self-assembly by turbidity and other techniques. *Methods Enzymol.* 130:47–59.
22. Padrick, S. B., and A. D. Miranker. 2002. Islet amyloid: phase partitioning and secondary nucleation are central to the mechanism of fibrillogenesis. *Biochemistry*. 41:4694–4703.
23. Chen, S. M., F. A. Ferrone, and R. Wetzel. 2002. Huntington's disease age-of-onset linked to polyglutamine aggregation nucleation. *Proc. Natl. Acad. Sci. USA*. 99:11884–11889.
24. Modler, A. J., K. Gast, G. Lutsch, and G. Damaschun. 2003. Assembly of amyloid protofibrils via critical oligomers: a novel pathway of amyloid formation. *J. Mol. Biol.* 325:135–148.
25. Collins, S. R., A. Douglass, R. D. Vale, and J. S. Weissman. 2004. Mechanism of prion propagation: amyloid growth occurs by monomer addition. *PLoS Biol.* 2:1582–1590.
26. Ignatova, Z., and L. M. Gierasch. 2005. Aggregation of a slow-folding mutant of a β-clam protein proceeds through a monomeric nucleus. *Biochemistry*. 44:7266–7274.
27. Ferrone, F. A. 1992. Sickle hemoglobin polymerization: the relationship between kinetics and pathophysiology. *Clin. Hemorheol.* 12: 163–175.
28. Masel, J., V. A. Jansen, and M. A. Nowak. 1999. Quantifying the kinetic parameters of prion replication. *Biophys. Chem.* 77: 139–152.
29. Masel, J., and V. A. Jansen. 2000. Designing drugs to stop the formation of prion aggregates and other amyloids. *Biophys. Chem.* 88:47–59.
30. Cohen, F. E., and J. W. Kelly. 2003. Therapeutic approaches to protein-misfolding diseases. *Nature*. 426:905–909.
31. Buxbaum, J. N. 2003. Diseases of protein conformation: what do in vitro experiments tell us about in vivo diseases? *Trends Biochem. Sci.* 28:585–592.
32. Everett, D. H. 1986. Some thermodynamic aspects of aggregation phenomena with special reference to micellization. *Coll. Surf.* 21: 41–53.
33. Wegner, A., and J. Engel. 1975. Kinetics of cooperative association of actin to actin filaments. *Biophys. Chem.* 3:215–225.
34. Bishop, M. F., and F. A. Ferrone. 1984. Kinetics of nucleation-controlled polymerization: a perturbation treatment for use with a secondary pathway. *Biophys. J.* 46:631–644.
35. McCoy, B. J. 2001. Distribution kinetics modeling of nucleation, growth, and aggregation processes. *Ind. Eng. Chem. Res.* 40:5147–5154.
36. Berg, O. G., and P. H. von Hippel. 1985. Diffusion-controlled macromolecular interactions. *Annu. Rev. Biophys. Biophys. Chem.* 14: 131–160.
37. Janin, J. 1997. The kinetics of protein-protein recognition. *Proteins*. 28:153–161.
38. Schreiber, G. 2002. Kinetic studies of protein-protein interactions. *Curr. Opin. Struct. Biol.* 12:41–47.
39. Kodaka, M. 2004. Interpretation of concentration-dependence in aggregation kinetics. *Biophys. Chem.* 109:325–332.
40. Hill, T. L. 1983. Length dependence of rate constants for end-to-end association and dissociation of equilibrium linear aggregates. *Biophys. J.* 44:285–288.
41. Hill, T. L. 1987. Linear Aggregation Theory in Cell Biology. Springer-Verlag, Berlin.
42. Kasai, M., F. Oosawa, and S. Asakura. 1962. Cooperative nature of G-F transformation of actin. *Biochim. Biophys. Acta*. 57: 22–31.
43. Frieden, C. 1983. Polymerization of actin: mechanism of the Mg^{2+}-induced process at pH 8 and 20 C. *Proc. Natl. Acad. Sci. USA*. 80: 6513–6517.

44. Frieden, C., and D. W. Goddette. 1983. Polymerization of actin and actin-like systems: evaluation of the time course of polymerization in relation to the mechanism. *Biochemistry*. 22:5836–5843.

45. Tobacman, L. S., and E. D. Korn. 1983. The kinetics of actin nucleation and polymerization. *J. Biol. Chem.* 258:3207–3214.

46. Sept, D., and J. A. McCammon. 2001. Thermodynamics and kinetics of actin filament nucleation. *Biophys. J.* 81:667–674.

47. Wakabayashi, K., H. Hotani, and S. Asakura. 1969. Polymerization of *Salmonella* flagellin in presence of high concentrations of salts. *Biochim. Biophys. Acta*. 175:195–203.

48. Saville, B. 1971. On the use of ''concentration-time'' integrals in the solution of complex kinetic equations. *J. Phys. Chem.* 75:2215–2217.

49. Powers, E. T., and D. L. Powers. 2003. A perspective on mechanisms of protein tetramer formation. *Biophys. J.* 85:3587–3599.

50. von Smoluchowski, M. 1917. Versuch einer mathematischen Theorie der Koagulationskinetik kolloider Lösungen. *Z. Phys. Chem.* 92: 129–168.

51. Galina, H., and J. B. Lechowicz. 1998. Mean-field kinetic modeling of polymerization: the Smoluchowski coagulation equation. *Adv. Polym. Sci.* 137:135–172.